Astron. Astrophys. 329, 1111–1118 (1998)

ASTRONOMY
AND
ASTROPHYSICS

Coronal plasmoid dynamics

I. Dissipative MHD approach

C. Delannée[1], **S. Koutchmy**[1], **I.S. Veselovsky**[2], **and A.N. Zhukov**[2]

[1] CNRS, Institut d'Astrophysique de Paris, 98 bis, Boulevard Arago, F-75014 Paris, France
[2] Institute of Nuclear Physics, Moscow State University, 119899 Moscow, Russia

Received 8 July 1996 / Accepted 5 August 1997

Abstract. Energy and momentum balance equations of the dissipative MHD approach are applied to the coronal plasmoid phenomenon observed with the Canada-France-Hawaii Telescope during the July 11, 1991 total solar eclipse. The situation is marginal for the applicability of the MHD description,which has been used for orders of magnitude estimates of the governing physical parameters. Their analysis confirms the suggestion about the possibility for a relatively cold but rapidly moving plasma body to heat the corona through dissipative viscous effects. It also shows that magnetic stresses, gas pressure gradients and viscous drags by the fast plasma flows from the chromosphere are viable candidates to lift the plasmoid against the gravity force.

Key words: Sun: corona – Sun: magnetic fields – MHD

1. Introduction

The mass, momentum and energy transport processes in the solar corona are known to proceed at various space and time scales manifested as quasistationary and dynamical plasma structures and magnetic fields. The relative importance of the processes occurring at these scales in the general balance equations remains the main enigma of the solar corona. Mutual interactions between scales play an important role because of the nonlinear character of inhomogeneities, but the dominant scales are still elusive and represent a field of debates and studies. The purpose of this paper is to present experimental and theoretical evaluations of the governing physical parameters, which may be important for the dynamics of the coronal plasmoid observed during the July 11, 1991 total solar eclipse. Plasmoids have been theoretically considered in the literature in many instances (Pneuman 1986; Mullan 1990; Schlüter 1957; Raadu et al. 1987; Cargill & Pneuman 1986; Landau & Lifshitz 1982). These structures are most probably magnetic clouds with closed internal magnetic field lines. The heating of the corona and the acceleration of the solar wind may be related to this phenomenon. Because of this it could play an important role in the physics of the solar corona.

The event we are considering here has already been partly described in the previous work (Vial et al. 1992) concentrated on the description of the observations and first, mostly visual analysis of the results. Here we describe the physical state of the plasma within and around the observed plasmoid.

2. Brief description of observations

The sub-arcsec structure of an ejected plasmoid travelling through the inner corona was resolved during the July 11, 1991 total solar eclipse (Vial et al. 1992) at the prime focus of the 3.6 m aperture CFH telescope on Mauna Kea.

The phenomenon, see Fig. 1, has been observed with a video CCD camera and a narrow pass band filter which excludes the low excitation emission lines. The spatial resolution achieved in this observation is of the order of 0.6 arcsec (Koutchmy et al. 1993) as measured on the sharp limb of the Moon near the end of the time series. During the observation the plasmoid was situated at an average distance of 130 arcsec, i. e. 90 000 km, above the solar limb at EES, between several moderately active regions (Koutchmy et al. 1994b). The plasmoid was filmed during 210 s. It moved outwards more or less along a direction inclined with 30° to the solar vertical. Its visual shape changed in a time lapse of approximately 70 s.

Comparative analysis of coronographic H_α observations made at the Pic du Midi Observatory (11:00 UT) with the eclipse pictures obtained in Mexico (La Paz, 18:48 UT) indicates an active prominence existing for more than 6 hours in a region of about 110 degrees and located not too far from where the plasmoid was observed (Guetman et al. 1994). Fig. 2 shows a large field of view around the plasmoid. This image was taken one minute before the time series, i. e. at the beginning of the totality. A filter which includes H_α was used for them. There is clearly a lot of activity in the underlying regions. This leads us to make the assumption that the plasmoid could be produced as a result of a micro-surge or of a macro or giant spicule eruption.

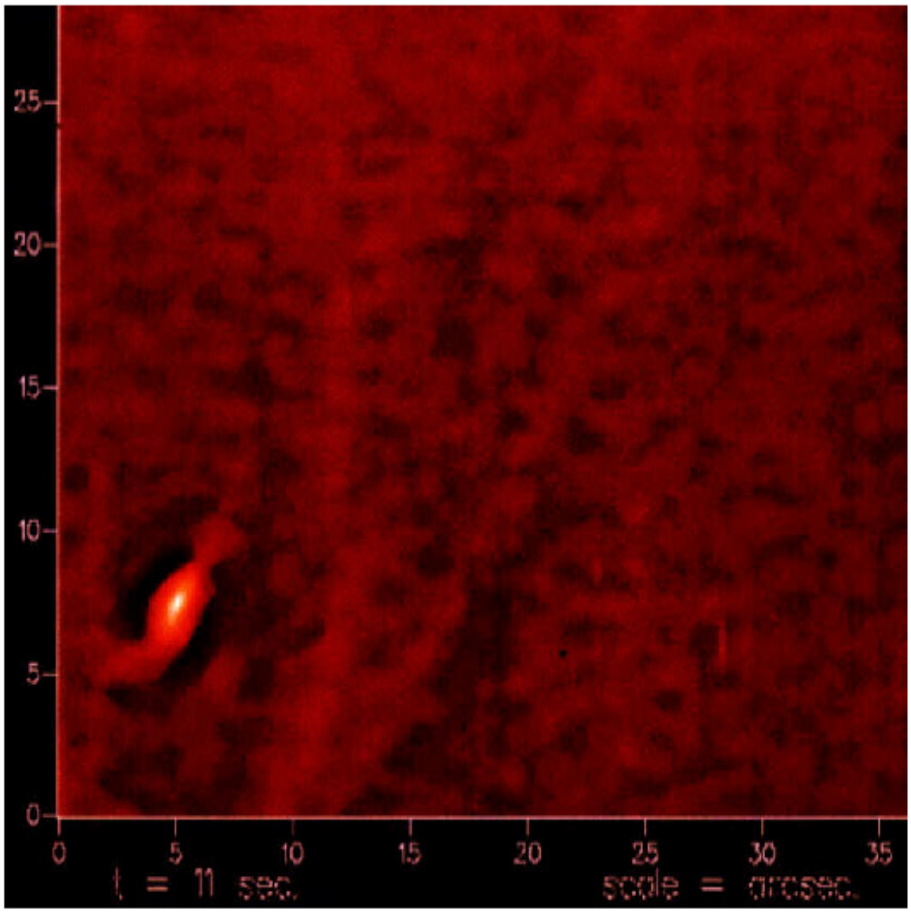

Fig. 1. A magnified and processed image coming from the beginning of the time series taken with the CCD camera put at the prime focus of the 3.6 m aperture CFHT. The background corona is removed. A filamentary structure is present in this image. The plasmoid is the brightest bulb, at the bottom left.

3. Evaluation of the relevant thermodynamical and MHD parameters

In this section we estimate the range of parameters which characterize the physical state of the plasmoid and of the surrounding corona by using both the available observations and standard models of the corona. For our consideration of the plasmoid's dynamics we will use MHD equations (the validity of this approach will be discussed later). The physical parameters inside and outside the plasmoid are summarized in Tables 1–3.

3.1. Geometries

The characteristic scale of the plasmoid was of order of 1500 km, as it was seen on the first images. The intensity profile of the plasmoid could be represented as a Gaussian function. The full width at half maximum of the intensity profile gives us the scale of the dominant intensity in the plasmoid. It was found of order of 600 km.

The real 3D geometry of the plasmoid is not known because we do not know its dimension along the line of sight. We shall make the usual hypothesis that it is of the same order as the two other dimensions. However, some parts of the plasmoid may be invisible to us and the possibility that the plasmoid has the shape of a long thread or of a loop which was placed along the viewing direction can not be completely excluded. The brightness of the plasmoid varies inversly to the square of the dimension, if the total mass of the plasmoid remains constant. Since the brightness of the plasmoid is close to the noise level, moderate variations in its dimensions can make it impossible to detect. The shape of the plasmoid changes during the time sequence and at the end it seems to disappear. This variation in brightness can be interpreted as the rotation of a thin filament with respect to the line of sight or the expansion (contraction) of a spherical blob of plasma.

3.2. Proper motion

The velocity of the plasmoid as a function of time has been obtained with a digital image processing using the correlation tracking algorithm (November & Simon 1988). The values of the bulk velocity of the plasmoid were 76 km s^{-1} at the beginning of the sequence and 43 km s^{-1} at the end of it (Delannée & Koutchmy 1996). It is not possible to determine any velocity field inside the plasmoid. The results of a previous paper (Koutchmy et al. 1994b) based on a rough analysis of observational velocity maps and indicating a reversal velocity inside the plasmoid appear to be too optimistic. After several re-analyses, we found that edge effects due to the strong brightness gradients at the boundaries of the plasmoid considerably affect the results.

Fig. 2. Large field of view image of the region surrounding the plasmoid during the eclipse, taken half a minute before the beginning of the time series with a red filter which includes the H_α line. The plasmoid is located at the head of the arrow, above an active region and between helmet streamers. From an original image obtained in the dome of the CFHT by J.P. Zimmermann.

3.3. Temperature

We can not precisely determine the temperature and the ionization degrees from the images. A filter with the pass band 7 nm at 638 $\pm$ 4 nm was used in front of the CCD camera. The FeX emission line which is situated in this pass band is invisible on the images of the plasmoid, so the light is only due to the Thomson scaterring. The plasmoid was ejected from the chromosphere and has not yet reached the coronal temperature. As the plasmoid was seen just one minute before the start of the film still emitting a small amount of H_α, we assume that the hydrogen in the plasmoid is fully ionized and the helium only partly. So, we estimate that the plasmoid temperature is the temperature needed to ionize the helium: T_1 = 2 10^4 K. The surrounding corona is supposed to be at the mean coronal temperature: T_2 = 2 10^6 K. The radiative balance will be considered in the forthcoming paper.

3.4. Densities

The estimates of densities inside and outside the plasmoid are very uncertain. We have used two independent methods both based on photographic photometry. The first one used the sequence of images obtained with the CCD camera: we measured the brightness of the plasmoid relative to that of the neighbouring corona ($\Delta I/I$) at the begining of the time series, see Fig. 1. We assume that the emitted light is due only to the Thomson scaterring. Hence, the brightness ratio is related to the electron density ratio by

$$\frac{\Delta I}{I} = \frac{\Delta n_{\rm e1}}{< n_{\rm e2} >} \frac{l_1}{L(h)}, \quad (1)$$

where l_1 is the dimension of the plasmoid, $L(h)$ = 10^5 km is the effective integration length in the background corona along the line of sight depending on the height h above the solar limb (November & Koutchmy 1996), $n_{\rm e1}$ is the electron density inside the plasmoid and $< n_{\rm e2} >$ is the average electron density of the corona at the corresponding height. If we take for the coronal density the standard value at the height of the plasmoid (Allen 1976), we obtain then $n_{\rm e1}$= 3 10^9 cm^{-3} and $< n_{\rm e2} >$= 3 10^8 cm^{-3}.

The second method we used is based on large field of view images. We have measured the signal coming from the plasmoid and the nearby region of the corona with a green continuum filter. Images of stars served for absolute calibration. This allowed us, using the method described by Lebecq et al. (1984), to obtain absolute estimates of the plasmoid mass as well as that of the density of the surrounding corona which are in rough agreement with the previous estimates.

3.5. Magnetic field

There is no data about the local coronal magnetic field in this region during the eclipse. Hence, we do not know its values inside and outside the plasmoid and we can only estimate the

Table 1. The physical parameters inside and outside the plasmoid

physical quantity	designation	unit	inside	outside
magnetic field	B	G	2	1
particle number density	n	cm^{-3}	$3\ 10^9$	$3\ 10^8$
mass density	ρ	$g\ cm^{-3}$	$5\ 10^{-15}$	$5\ 10^{-16}$
temperature	T	K	$2\ 10^4$	$2\ 10^6$
bulk velocity	v	$km\ s^{-1}$	43-76	?
sound speed	c_s	$km\ s^{-1}$	15	150
proton thermal velocity	v_{Tp}	$km\ s^{-1}$	22	220
electron thermal velocity	v_{Te}	$km\ s^{-1}$	950	$9.5\ 10^3$
Alfvén velocity	v_A	$km\ s^{-1}$	80	130
electron Langmuir frequency	ω_0	s^{-1}	$3\ 10^9$	10^9
proton Larmor frequency	ω_{Hp}	s^{-1}	$2\ 10^4$	10^4
electron Larmor frequency	ω_{He}	s^{-1}	$4\ 10^7$	$2\ 10^7$
proton Larmor radius	r_{Hp}	m	1.1	22
electron Larmor radius	r_{He}	m	0.03	0.5
Debye radius	r_D	cm	0.018	0.6
proton mean free path	λ_p	km	0.019	1200
electron mean free path	λ_e	km	0.019	1200
proton Coulomb frequency	ν_{pp}	s^{-1}	1200	0.19
electron Coulomb frequency	ν_{ee}	s^{-1}	$5\ 10^4$	8
viscosity	η	$g\ cm^{-1}\ s^{-1}$	$6.5\ 10^{-6}$	0.4
kinematic viscosity	ν	$cm^2\ s^{-1}$	$1.3\ 10^9$	$8\ 10^{14}$
heat conductivity	κ	$cm^{-1}\ s^{-1}$	$6\ 10^{20}$	$3.6\ 10^{25}$
temperature conductivity	χ	$cm^2\ s^{-1}$	$2\ 10^{11}$	$1.2\ 10^{17}$
electric conductivity	σ	s^{-1}	$3\ 10^{13}$	$2\ 10^{16}$

Table 2. The dimensionless parameters of the equation of motion and energy balance equation

dimensionless number	definition	designation	inside[a]	referring to the corona
Strouhal	vt/l	S	$(0.02 – 0.14)v_{ins}$	0.9 – 11
Mach	v/c_s	M	$v_{ins}/15$	0.3 – 0.5
Mach-Alfvén	v/v_A	M_A	$v_{ins}/80$	0.3 – 0.6
Reynolds	lv/ν	Re	$12000\ v_{ins}$	0.8 – 1.4
Prandtl	ν/χ	Pr	0.007	0.007
magnetic Reynolds	$4\pi\sigma lv/c^2$	Re_m	$6\ 10^6\ v_{ins}$	$(2 – 3)\ 10^{11}$
Knudsen	λ/l	Kn	$1.3\ 10^{-5}$	0.8
"velocity/emission"	$\frac{E_{kin}}{E_{rad}}\frac{\tau_{rad}}{t}$	Ve	10^2	–
Froude	v^2/gl	Fr	$0.003\ v_{ins}^2$	6 – 17
plasma parameter	$8\pi p/B^2$	β	0.1	4

[a] In this column v_{ins} must be taken in $km\ s^{-1}$.

magnetic field under the assumptions of potential or force-free magnetic field in the corona (Hoeksema & Suess 1990; Pätzold et al. 1987; Duvall et al. 1979), and of pressure balance between the plasmoid and the corona; the lack of visible strong expansion or contraction of the plasmoid as a whole means that it is roughly in pressure equilibrium:

$$p_1 + \frac{B_1^2}{8\pi} = p_2 + \frac{B_2^2}{8\pi}. \quad (2)$$

Estimated values are $B_1 = 2$ G, $B_2 = 1$ G (Koutchmy et al. 1994b).

4. Driving forces

The driving forces of the plasmoid appear in the right-hand side of the equation of motion:

Table 3. Some bulk parameters of the plasmoid

quantity	designation	unit	value
length	l	Mm	1.5
volume	V	cm^3	1.8 10^{24}
mass	m	g	9 10^9
magnetic moment	μ	G cm^3	3 10^{24}
magnetic flux	Φ	G cm^2	7 10^{16}
internal energy (mainly magnetic)	$E_{\rm int}$	erg	3 10^{23}
kinetic energy	$E_{\rm kin}$	erg	(0.8 – 2.6) 10^{23}
electric current	I	A	2 10^9

$$\rho(\frac{\partial \boldsymbol{v}}{\partial t} + (\boldsymbol{v}\boldsymbol{\nabla})\boldsymbol{v}) = -\boldsymbol{\nabla}P + \frac{1}{c}(\boldsymbol{J}\wedge\boldsymbol{B}) + \eta[\triangle\boldsymbol{v} + \frac{1}{3}\boldsymbol{\nabla}(\boldsymbol{\nabla}\boldsymbol{v})] - \frac{\rho M_\odot G}{r^3}\boldsymbol{r} + \boldsymbol{F}_r. \quad (3)$$

These forces are respectively: gas pressure gradient, Ampere force, frictional drag of the plasmoid in the external flow, gravity force and, finally not excluded, the radiation pressure represented by the last term in Eq. (3) ($\boldsymbol{F}_r$). The ordering between the magnitudes of these forces is not completely clear because of the poor knowledge of the physical parameters of the plasmoid and the surrounding corona, we can only guess about their role. We are trying to find what forces can expel the plasmoid.

4.1. Strouhal number

The dimensionless Strouhal number is the ratio of two terms in the left-hand side of Eq. (3): $S_2 = v_1 t/l_1 = 0.9-11$, where v_1 is the characteristic velocity, $t = 30-70$ s; the upper value being the characteristic time of the visual shape changes and the lower value being the characteristic time of the velocities variations.

The Strouhal number determines the role of the time variations. At the beginning of the sequence the plasmoid is a quasistationary phenomenon ($S_2 \sim 10$) and the first term in the left-hand side of Eq. (3) may be neglected as a first approximation. As the time goes, the plasmoid becomes a nonstationary phenomenon ($S_2 \sim 1$).

4.2. Gravity

The gravity force tends to pull the plasmoid back towards the chromosphere since the mass density of the plasmoid is greater than the mass density of the corona, but the Froude number $Fr = 6-17$, so gravity plays only small dynamical role.

4.3. Radiative pressure

The absorption and the scattering of the solar radiation flux from the photosphere by local density enhancements in the solar chromosphere and corona inhomogeneities in approximate magnetohydrostatic equilibrium may be one of the factors which may disrupt this equilibrium and accelerate the matter outwards. But the estimates of the Thomson scattering, Paschen and red line Fe X emissions (Vial et al. 1992) show very low efficiency of these mechanisms for the plasma acceleration.

Indeed, the energy needed to accelerate the plasmoid is equal to $E_{\rm kinetic} = mv_1^2/2 = 2.6\ 10^{23}$ erg, where the mass of the plasmoid is $m = \pi m_{\rm p} n_1 l_1^3/6 = 9\ 10^9$ g for $n_1 = 3\ 10^9$ cm^{-3} (equal to the electron density), $m_{\rm p}$ is the proton mass.

The energy available from the solar radiation pressure $P_\odot = 2.1$ erg cm^{-3} at the distance $\Delta r = 9\ 10^4$ km from the photosphere to the region where the plasmoid was observed is equal to $E_{\rm radiation} = \pi l_1^2 P_\odot \Delta r \approx 10^{27}$ erg. The energy transported to the plasmoid is: $E_{\rm radiation}\sigma l_1 n_1 \approx 4\ 10^{20}$ erg with σ is the Thomson scattering cross section ($\sigma = 6.6\ 10^{-25}$ cm^2). This energy is three orders less than the kinetic energy. The radiation pressure probably plays a negligible role in the phenomenon.

4.4. Gas pressure gradient

The Mach numbers are $M_1 = v_{\rm ins}/c_{\rm s1} = v_{\rm ins}/15$ and $M_2 = v_1/c_{\rm s2} = 0.3-0.5$, where $v_{\rm ins}$ (in km s^{-1}) is the velocity of the plasma flows (turbulence, currents) inside the plasmoid, $c_{\rm s}$ is the sound velocity. Gas pressure gradient may be important because of the nearly sonic plasmoid motion.

4.5. Viscous drags

The region underlying the plasmoid was a rather active one for several days. Red and blue H_α shifts of about 0.9 Å were observed in this region on July 12 (Solar Geophysical Data) within an active prominence (Guetman et al. 1994). These flows may have pushed the plasmoid from the chromospheric layers.

The estimated proton and electron mean free paths against Coulomb collisions are 19 m inside the plasmoid and 1.2 Mm outside it. Corresponding Knudsen numbers are $Kn_1 = \lambda_{\rm p1}/l_1 = 1.3\ 10^{-5}$ and $Kn_2 = \lambda_{\rm p2}/l_1 = 0.8$ respectively, which give Reynolds numbers $Re_1 = l_1 v_{\rm ins}/\nu_1$=1.2 10^4 $v_{\rm ins}$ ($v_{\rm ins}$ is in km s^{-1}) and $Re_2 = l_1 v_1/\nu_2 = 0.8-1.4$ in the corona. The value $Kn_2 \sim 1$ indicates that the MHD approach is only marginally applicable for consideration of the plasmoid interaction with the surrounding medium (see Sect. 6).

The Reynolds number inside the plasmoid is more difficult to estimate because we do not know the velocity inside the plasmoid and the characteristic scale of the turbulent cells. The biggest length scale we can estimate is equal to the plasmoid dimension, but the turbulent cells inside the plasmoid may be much smaller than this dimension. As the scale becomes smaller, the Reynolds number becomes smaller and the effectiveness of the viscous friction greater. The variation of the velocity produce the same effect. If we take the length scale equal to the plasmoid dimension, the velocity have to be unrealistically small (8 cm s^{-1}) to neglect the turbulence and the heating by convection.

This means that the viscous friction inside the plasmoid is negligible and a turbulent regime under frequent collisions is possible there. The flow around the plasmoid is laminar, because the Reynolds number here is approximately equal to 1. In this sense the internal flows inside the plasmoid may be uncoupled and independent from the external flow. Hence, the sign of the internal vortex rotating inside the plasmoid may be not a good indicator of presence or absence of the viscous drag and probably says something only about conditions inside the plasmoid and not about its interaction with the surrounding medium.

4.6. Magnetic force

Protons and electrons Larmor frequencies in a magnetic field of 1 G in the corona are estimated to be 10^4 s^{-1} and 2 10^7 s^{-1} respectively. Inside the plasmoid the protons and electrons Larmor frequencies are estimated to be 2 10^4 s^{-1} and 4 10^7 s^{-1} respectively. The corresponding Larmor radii outside are 22 m and 0.5 m. These radii are about 20 times smaller inside the plasmoid, i. e. 1.1 m and 0.03 m respectively. Magnetic forces dominate over the gas pressure inside the plasmoid because of low β there.

The Mach-Alfvén number is M_{A2} = 0.3 – 0.6 outside the plasmoid and inside $M_{A1} = v_{ins}/80$, if we take v_{ins} in km s^{-1}. The corresponding magnetic Reynolds numbers are $Re_{m2} = (2-3)10^{11}$ and $Re_{m1} = 6\ 10^6\ v_{ins}$ (v_{ins} is again in km s^{-1}). Therefore the Ohmic dissipation seems to be small. The estimated magnetic flux of the plasmoid ($\sim 7\ 10^{16}$ G cm^2) is in coincidence with the observed peak in the flux distribution of intranetwork magnetic elements (Wang et al. 1995a, b).

5. Energy balance

The standard energy equation may be written as follows:

$$\frac{\partial}{\partial t}(\rho u + \rho\frac{v^2}{2}) + \frac{\partial}{\partial x_i}(\rho v_i w + \rho v_i\frac{v^2}{2} - v_k\sigma'_{ik} - \kappa\frac{\partial T}{\partial x_i} + \frac{1}{4\pi}e_{ikl}e_{lmn}v_m B_k B_n + \frac{c}{4\pi\sigma}e_{ikl}J_k B_l) = -L + A, \qquad (4)$$

where L represents local energy gains and losses due to atomic processes (radiation, ionization, excitation etc.), $A = -\frac{\rho M_\odot G}{r^3}\boldsymbol{rv}$ is the work of external (gravity) forces, σ'_{ik} is the viscous tensor, u is the internal energy, w is the enthalpy.

Proton Coulomb collision frequencies are about 1200 s^{-1} inside and 0.19 s^{-1} outside the plasmoid, and electron Coulomb collision frequencies are about 5 10^4 s^{-1} inside and 8 s^{-1} outside the plasmoid. Protons and electrons are collision dominated both inside and outside the plasmoid.

However, all transport coefficients are strongly modified by the presence of the magnetic field inside and outside the plasmoid. We estimate the transport coefficients along the magnetic field as follows: the kinematic viscosity is 1.3 10^9 cm^2 s^{-1} inside and 8 10^{14} cm^2 s^{-1} outside the plasmoid; the temperature conductivity is 2 10^{11} cm^2 s^{-1} inside and 1.2 10^{17} cm^2 s^{-1} outside; electric conductivity $\sigma \approx 3\ 10^{13}$ s^{-1} inside and 2 10^{16} s^{-1} outside. Transport coefficients across the magnetic field are several orders smaller than the corresponding coefficients along the field. All Coulomb collision frequencies, transport coefficients and mean free paths were estimated via formulae from Braginsky (1963).

In addition to the standard dimensionless MHD numbers (i. e. S, M, M_A, Re, Re_m, Pr, Fr) and their combinations in the energy balance equation (4), a specific dimensionless number should be introduced to characterize the relative role of the radiative gains, losses and other atomic processes (the term L in Eq. (4)). This dimensionless parameter, Ve, is very interesting to consider for our purposes. It is introduced as follows.

Comparing the radiative term with the kinetic energy flux of the plasma flow, we obtain a so-called "velocity/emission" dimensionless number Ve, defined as $Ve = (\partial E_{kin}/\partial t)(\partial E_{rad}/\partial t)^{-1}$. Using the estimates of the free-free and free-bound radiation losses (see e. g. Cox & Tucker 1969; Priest 1982) , we obtain $Ve_1 \sim 10^2$. This means that the atomic and radiative processes are not essential in the energy balance of the plasmoid, when compared with its kinetic energy.

6. Discussion

The plasmoid motion is nearly quasistationary because most of the time $S_2 > 1$. Equation (2) of the pressure balance between the plasmoid and the surrounding corona is approximately fulfilled. But the structure is probably better approximated by a travelling MHD perturbation like an Alfvén soliton (toroidal magnetic cloud) because $M_A \approx 0.3 - 0.6$.

The internal energy of the plasmoid (magnetic and kinetic) is not conserved during the motion: the viscous friction represents an important part of the plasmoid interaction with the background coronal plasma because $Re_2 \approx 1$ in the external region. The Joule heating is rather small. Hence, the viscous dissipation takes place which leads to the transformation of the plasmoid kinetic energy to the heat absorbed mainly by the background coronal plasma (and not by the plasmoid) because of its extremely high heat conductivity. Only a part of this heat is absorbed by the moving plasmoid during the active stage when its velocity appreciably differs from the velocity of the surrounding plasma, because of the low temperature conductivity of the cold plasmoid body. Hence, kinetic and magnetic energies of the plasmoid are absorbed via the viscous dissipation by the corona. This heating process is possible only because of the

lack of the equilibrium which is manifested as an inhomogeneity and non stationarity of the plasma motion driven by Ampere forces. The thickness of the viscous layer may be estimated as: $X \sim \beta M \lambda_{\rm p} \sim (1-2)\lambda_{\rm p} \simeq 1.2-2.4$ Mm (this estimate follows from the balance between the terms $v\sigma^{'}$ and $vB^2/4\pi$ in the energy balance equation (4)). Strong convective motions and $T_2 \simeq$ const are anticipated in the viscous layer between the plasmoid and the background plasma. The viscous stopping time of the plasmoid estimated from the equation of motion (3) is about $t \sim XM^2\beta/v \simeq 10-32$ s.

After this characteristic time the plasmoid and the surrounding plasma are "viscously connected" one to other. The "viscously connected" plasmoid may be heated not only by the heat conductivity (which is small inside the plasmoid), but by the convection which is believed to be effective for large Reynolds number. It is difficult to estimate the heating time during this turbulent process, but this time should be larger than the "sonic time" $t \sim l/c_{\rm s1} \simeq 100$ s.

The solar corona is a dissipative medium. It is highly viscous and temperature conductive. For example, its viscosity ($\eta = 0.4$ g cm^{-1} s^{-1}) and its kinematic viscosity ($\nu = 8\ 10^{14}$ cm^2 s^{-1}) are orders of magnitude greater than the corresponding numbers in the same units for usual media like water ($\eta = 10^{-2}$ g cm^{-1} s^{-1} , $\nu = 10^{-2}$cm^2 s^{-1}) or air ($\eta = 1.8\ 10^{-4}$ g cm^{-1} s^{-1}, $\nu = 0.15$ cm^2 s^{-1}) under standard conditions ($T = 300$ K). Hence, we found a support to the view that the solar corona could be heated by viscous dissipation (Shklovsky 1962).

We have used the MHD approach for our investigation of the plasmoid's interaction with the surrounding medium although $Kn_2 \sim 1$. Strictly speaking, this case should be investigated through the general kinetic consideration, which leads to MHD if $Kn \ll 1$ and to collisionless kinetics if $Kn \gg 1$. The case $Kn \sim 1$ is hard to investigate analytically. However, a simple example permits to anticipate that the MHD approach to the plasmoid dynamics is a possible way of obtaining rough order of magnitude estimates needed for us.

Let us consider a solid spherical body with radius R moving through the gas. If the mean free path of the gas particles λ is sufficiently small ($\lambda \ll R$, i. e. $Kn \ll 1$) and Reynolds number is also small, we can obtain the resistive force according to the Stokes formula: $F = 6\pi\eta VR \sim \eta VR$ (Landau & Lifshitz 1988), where V is the velocity of the body,

$$\eta \sim \rho v_{\rm T} \lambda \sim \rho v_{\rm T} R Kn \tag{5}$$

is the viscosity coefficient, ρ is the gas density, $v_{\rm T}$ is the mean thermal velocity of the gas particles. In the opposite case $\lambda \gg R$ ($Kn \gg 1$), if the velocity V is not hypersonic, the resistive force reads as $F \sim VR^2\rho v_{\rm T}$ (Lifshitz & Pitaevsky 1979). This formula can be rewritten as $F \sim \rho v_{\rm T} RVR$. Comparing two expressions for F derived in the cases $Kn \ll 1$ and $Kn \gg 1$, we can write formally the viscosity coefficient in the case $Kn \gg 1$:

$$\eta \sim \rho v_{\rm T} R. \tag{6}$$

The formulae (5) and (6), when extrapolated into the region $R \sim \lambda$, give the same value $\eta \sim \rho v_{\rm T} R$ because of $Kn \sim 1$. So, in both approaches (MHD and collisionless kinetics) the resistive force is characterized by the same coefficient. Analogous considerations could be performed for other transport processes. This validates our use of the dissipative MHD approaches for obtaining order of magnitude estimates in this paper.

An interesting question about the role of collisionless kinetic processes at the internal plasma degrees of freedom (different electromagnetic waves and oscillations inside and outside the plasmoid) is open and beyond the scope of this paper. These processes are often supposed to be important in coronal heating and solar wind acceleration. We do not exclude the possibility that small-scale collisionless processes are important for the coronal plasmoid too. This would mean a kinetic regime with a strong plasma turbulence, which should have some observational manifestations in the radiation, larger scale structure and dynamics of the plasmoid.

7. Conclusions

Magnetic forces, gas pressure gradient and fast flows from the chromosphere are viable candidates to serve as lifting factors for the plasmoid. This conclusion is supported by other observational and theoretical works (Golub 1992; Haerendel 1992; Veselovsky 1991)

At present we cannot definitely indicate the locally dominant lifting force because of the poor knowledge of the plasma parameters inside and outside the plasmoid. This question should be resolved using new observations of all governing physical parameters in the corona. The SOHO mission will hopefully bring new measurements.

Nonstationary and inhomogeneous vertical and horizontal convective motions driven by magnetic forces and gas pressure gradient partially dissipate via viscous friction in the solar corona. Under good frozeness conditions (high magnetic Reynolds numbers) this leads to the non equilibrium situations, when cold moving plasma transports its magnetic and kinetic energy to the hotter surrounding plasma. We suggest that the coronal plasmoid represents an example of such a heating process. Naturally, other mechanisms suggested to explain the coronal heating could be operative, especially taking into account a multiscale nature of coronal structures.

We have considered the plasmoid mainly as a one-dimensional phenomenon dominated by its visible dimension of about 1 Mm and have obtained some indications on the role of other (larger and smaller) scales inside and outside its volume. The interplay between different space and time scales needs additional investigations.

Acknowledgements. The paper was partially prepared when C. Delannée visited the Moscow State University. The work of I. S. Veselovsky is supported through the RFBR grant 95-02-06074-a. This research is also partly supported by the NATO. We thank A. Mangeney for very useful discussion and suggestions.

References

Allen C.W., 1976, Astrophysical Quantities. Athlone Press

Braginsky S.I., 1963, Transport Phenomena in Plasma. In: Leontovich M.A. (ed.) Plasma Theory Questions, vol. 1. Gosatomizdat, Moscow (in Russian)
Cox D.P., Tucker W.H., 1969, ApJ 157, 1157
Cargill P.J., Pneuman G.W., 1986, ApJ 307, 820
Delannée C., Koutchmy S., 1996, C.R. Acad. Sci. Paris, t. 322, Série II b, 79
Duvall T.L., Scherrer P.L., Svalgaard L., Wilcox J., 1979, Solar Physics 61, 233
Golub L., 1992. In: Giampapa S., Booklinder J.A. (eds.) Seventh Cambridge Workshop on Cool Stars, Stellar Systems and the Sun, ASP Conference Series, vol. 26, p. 193
Guetman F.I., Kim I.S., Bücher A., Druzhinin C.A., Noëns J.-C., Salahutdinov R.T., Semenikhin A.A., Skomorovsky V.I., 1994. In: Rušin V., Heinzel P., Vial J.-C. (eds.) IAU Coll. 144 "Solar Coronal Structures". VEDA Pub, Co., Bratislava, p. 575
Haerendel G., 1992, Proceedings of the 26^{th} ESLAB Symposium, Ireland, ESA SP-346, p. 32
Hoeksema J.T., Suess S.T., 1990, Societa Astronomica Italiana 61, 485
Koutchmy S., Bouchard O., Mouette J., Koutchmy O., 1993, Solar Physics 148, 169
Koutchmy S., Veselovsky I.S., 1994, Paper E2.2 presented at the 30^{th} COSPAR Scientific Assembly, Hamburg, Adv. Space Res. (in press)
Koutchmy S., Belmahdi M., Coulter R.L. et al., 1994, A&A 281, 249
Koutchmy S., Bouchard O., Grib S.A. et al., 1994, SOHO III Conf., ESA SP-373, p. 139
Landau L.D., Lifshitz E.M., 1982, Electrodynamics of Continuous Media. Nauka, Moscow (in Russian)
Landau L.D., Lifshitz E.M., 1988, Hydrodynamics. Nauka, Moscow(in Russian)
Lebecq C., Koutchmy S., Stellmacher G., 1984, A&A 152, 157
Lifshitz E.M., Pitaevsky L.P., 1979, Physical Kinetics. Nauka, Moscow (in Russian)
November L.J., Simon G.W., 1988, ApJ 333, 427
November L.J., Koutchmy S., 1996, ApJ 466, 512
Mullan D.J., 1990, A&A 232, 520
Pätzold M., Bird M.K., Volland H., 1987, Solar Physics 109, 91
Pneuman G.W., 1986, Space Sci. Rev. 43, 105
Priest E.R., 1982, Solar Magnetohydrodynamics. Reidel, Dordrecht
Raadu M.A., Malherbe J.M., Schmieder B.S., Mein P., 1987, Solar Physics 109, 59
Schlüter A., 1957. In: Hulst H.C. Van der (ed.) IAU Symposium 4, Radio Astronomy. Cambridge University Press, Cambridge, p. 356
Shklovsky I.S., 1962, Physics on the Solar Corona. Phys. Mathem. State Publ. Co., Moscow (in Russian)
Solar Geophysical Data ♯569, part II, 1992
Veselovsky I.S., 1991, Nonstationary Sub and Super-Alfvenic Motions in the Solar Corona. Solnechnye Dannye, N 11, 89 (in Russian)
Veselovsky I.S., 1996, Nearly sonic and transsonic convective motions in the solar atmosphere related to the solar wind origin. In: Winterhalter D. et al. (eds.) Solar Wind Eight: International Solar Wind 8 Conference. AIP Press, Woodbury, New York, p. 161
Vial J.-C., Koutchmy S., and the CFHT team, 1992, Proceedings of an ESA Workshop on Solar Physics and Astrophysics at Interferometric Resolution. Paris, p. 87
Wang Y., Noyes R.W., Tarbel T.D., Title A.M., 1995, ApJ 447, 419
Wang Y., Wang H., Tang F., Lee J.W., Zirin H., 1995, Solar Physics 160, 277

This article was processed by the author using Springer-Verlag LaTeX A&A style file *L-AA* version 3.